SANDIA REPORT
SAND2008-0330
Unlimited Release
Printed February 2008

Modeling and Simulation of Blast-Induced, Early-Time Intracranial Wave Physics leading to Traumatic Brain Injury

Paul A. Taylor and Corey C. Ford

Prepared by
Sandia National Laboratories
Albuquerque, New Mexico 87185 and Livermore, California 94550

Sandia is a multiprogram laboratory operated by Sandia Corporation,
a Lockheed Martin Company, for the United States Department of Energy's
National Nuclear Security Administration under Contract DE-AC04-94AL85000.

Issued by Sandia National Laboratories, operated for the United States Department of Energy by Sandia Corporation.

Available to DOE and DOE contractors from
U.S. Department of Energy
Office of Scientific and Technical Information
P.O. Box 62
Oak Ridge, TN 37831

Telephone: (865) 576-8401
Facsimile: (865) 576-5728
E-Mail: reports@adonis.osti.gov
Online ordering: http://www.osti.gov/bridge

Available to the public from
U.S. Department of Commerce
National Technical Information Service
5285 Port Royal Rd.
Springfield, VA 22161

Telephone: (800) 553-6847
Facsimile: (703) 605-6900
E-Mail: orders@ntis.fedworld.gov
Online order: http://www.ntis.gov/help/ordermethods.asp?loc=7-4-0#online

SAND2008-0330
Unlimited Release
Printed February 2008

Modeling and Simulation of Blast-Induced, Early-Time Intracranial Wave Physics leading to Traumatic Brain Injury

Paul A. Taylor
Multiscale Dynamic Materials Modeling Department
Sandia National Laboratories
Albuquerque, NM 87185

Corey C. Ford, MD, PhD
Department of Neurology
University of New Mexico Health Sciences Center
Albuquerque, NM 87131-0001

Abstract

The objective of this modeling and simulation study was to establish the role of stress wave interactions in the genesis of traumatic brain injury (TBI) from exposure to explosive blast. A high resolution (1 mm^3 voxels), 5 material model of the human head was created by segmentation of color cryosections from the Visible Human Female dataset. Tissue material properties were assigned from literature values. The model was inserted into the shock physics wave code, CTH, and subjected to a simulated blast wave of 1.3 MPa (13 bars) peak pressure from anterior, posterior and lateral directions. Three dimensional plots of maximum pressure, volumetric tension, and deviatoric (shear) stress demonstrated significant differences related to the incident blast geometry. In particular, the calculations revealed focal brain regions of elevated pressure and deviatoric (shear) stress within the first 2 milliseconds of blast exposure. Calculated maximum levels of 15 KPa deviatoric, 3.3 MPa pressure, and 0.8 MPa volumetric tension were observed before the onset of significant head accelerations. Over a 2 msec time course, the head model moved only 1 mm in response to the blast loading. Doubling the blast strength changed the resulting intracranial stress magnitudes but not their distribution. We conclude that stress localization, due to early time wave interactions, may contribute to the development of multifocal axonal injury underlying TBI. We propose that a contribution to traumatic brain injury from blast exposure, and most likely blunt impact, can occur on a time scale shorter than previous model predictions and before the onset of linear or rotational accelerations traditionally associated with the development of TBI.

Acknowledgements

The authors would like to express their gratitude to Michael Dwyer, Director of Technical Imaging Development, Buffalo Neuroimaging Analysis Center (BNAC), Jacobs Neurological Institute, University at Buffalo, for segmenting the color cryosections for the head model used in this study.

We would also like to thank Dr. M. E. Kipp for his insightful technical review of the manuscript.

Contents

Figures

This Page Intentionally Left Blank

Modeling and Simulation of Blast-Induced, Early-Time Intracranial Wave Physics leading to Traumatic Brain Injury

Introduction

The yearly incidence of traumatic brain injuries (TBI) in the United States has been estimated at 1.4 million people, with 50,000 deaths and 235,000 hospitalizations [1]. Military personnel and civilians can incur TBI as a consequence of explosive blasts and in recent wars the incidence of such injuries has increased dramatically. This increase can be attributed to the consequences of asymmetric warfare, where enemy combatants detonate improvised explosive devices targeting vehicles and exposed individuals and to improvements in armor and trauma evacuation and care allowing survival of previously fatal injuries. By the end of June, 2007, several thousand US soldiers fighting in Iraq had sustained TBI, 69% as a result of blasts [2;3]. Injuries sustained from blast exposure have been categorized into three major components, primary, secondary and tertiary [4]. Primary blast injury is associated with direct exposure of the head and body to the blast wave. In secondary blast injury, debris is accelerated into the individual, while in tertiary injury the victim is thrown into stationary objects by the blast. Both of the latter mechanisms are comparable to the mechanical trauma that has been the subject of decades of clinical, experimental and computational research. However, the role of primary blast exposure in the development of TBI remains less well understood [5]. Primary blast may induce linear and rotational cranial accelerations, but the sharp wave front of blast overpressure will also trigger complex wave motions, transmitted by the skull into the high water content viscoelastic brain.

Multiple, often coexisting pathologies can underlie the consequences of TBI, including easily visualized damage from contusions and intraparenchymal or extra-axial hemorrhages. However, at least one third of the deaths and poor outcomes of TBI are the result of traumatic axonal injury occurring at the microscopic level [6]. Most often referred to as diffuse axonal injury or DAI, this pathological finding actually defines a multifocal process that can be widespread throughout the white matter tracks and other areas of the brain [7]. DAI has been linked to dynamic deformations caused by linear and rotational accelerations [8-11]. In pig models rapid, non-impact, inertial loading produced multifocal axonal injury throughout the brain [12]. Studies of the brain after TBI have shown cytoskeletal disruptions, changes in membrane permeability and the development of axonal swelling that can be followed by axonal transections with terminal axon bulbs [9;13;14]. The long standing idea that the severed axons seen after TBI were the result of mechanical tearing has been replaced by the realization that most transected axons undergo a progressive, self-destruction sequence after the initial traumatic insult [15-18]. DAI has been demonstrated by histopathology in TBI of all severities and studies have inferred its presence by non-conventional MRI in brain injured patients with no other signs of damage on routine brain CT and MRI scans [19;20].

Can TBI occur without macroscopic damage and unassociated with large translational or rotational motions? Could complex wave action in the brain, after impact or blast, result in focal injury to axons and trigger the cascade of secondary events leading to transections and permanent neurological disabilities? Loss of consciousness and brain injury from assault with a blunt object may not involve significant head motion. The different mechanisms of TBI and the variable outcomes for patients with similar levels of apparent injury led us to examine the role of wave action in delivering mechanical energy to critical brain regions.

Our hypothesis in this study is that stress waves from blast exposure will transit and reflect within the intracranial contents of the head resulting in focal areas of elevated stress great enough to cause axonal injury. The primary focus of this paper is to explore the role of intracranial wave mechanics in the genesis of traumatic brain injury from blast.

Modeling and Simulation Methodology

Head Model

With the assistance of colleagues at the Buffalo Neurological Center in Buffalo, NY, we constructed a head model based on the segmentation of high resolution photographic data available from the Visible Human Project of the National Library of Medicine [21]. The photographic data consists of 0.33 mm thick axial slices of a cryogenically frozen human female. The axial slice image data was segmented using a pattern recognition algorithm applied to every third slice comprising the head above the mandible, resulting in a head model possessing a 1 mm cubic resolution for a total of 6,850,560 voxels (192x223x160). The slice segmentation data were assembled into a single file that was used to generate material geometry of the head model for our simulation wave code. The head model is comprised of skull bone, white and gray brain matter, cerebral spinal fluid (CSF), and air spacing representing the sinuses. Figure 1 displays representative images of the head model as it is defined within the wave code.

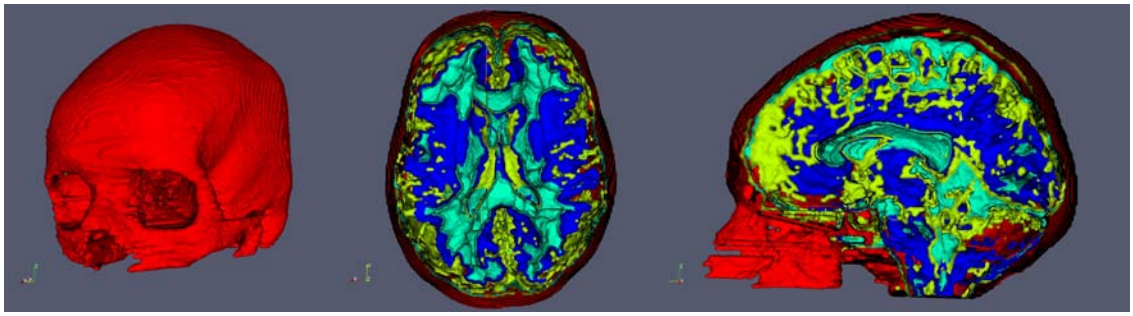

Figure 1. Head model. Color code: red = bone, light blue = white matter, dark blue = gray matter, yellow = cerebral spinal fluid (CSF). Voxel resolution: 1 cubic millimeter.

Material Models

Our simulation method incorporates equation-of-state and constitutive models representing the components of the head: skull bone, white and gray brain matter, cerebral spinal fluid (CSF), and air within sinuses. The skull is modeled as an isotropic, linear elastic, perfectly plastic material with a strain-to-failure fracture model based on data reported in the literature [22]. These properties are listed in Table 1. The white and gray matter are modeled as isotropic, compressible viscoelastic materials with properties adopted from those reported by Zhang et al. [23]. These tissues are represented by an elastic compressible equation of state model for the volumetric response and a generalized, three-term Maxwell viscoelastic model for deviatoric (shear) response. The time-dependent shear modulus of the brain tissue is represented by the equation

$$G(t) = G_\infty + (G_o - G_\infty)e^{-\beta \cdot t}, \quad (1)$$

where t denotes time, G_o is the short-term shear modulus, G_∞ is the long-term modulus, and β denotes the viscous decay constant. The material properties of the brain tissue are listed in Tables 1 and 2. The CSF and air are represented by nonlinear, tabular equation-of-state models that have been specifically designed for shock wave applications [24]. A region of air envelops the head in order to transmit the blast wave. The air employs the same tabular equation-of-state representation that is used to describe the air residing in the sinuses.

Table 1. Elastic material properties

	Density (g/cc)	Initial Bulk Modulus (GPa)	Poisson's Ratio	Yield Stress (MPa)	Strain to Failure (%)	Fracture Stress (MPa)
Skull	1.412	4.82	0.22	95	0.8	77.5
White Matter	1.04	2.37	0.49	--	--	--
Gray Matter	1.04	2.37	0.49	--	--	--

Table 2. Viscoelastic material properties

	Short-term Shear Modulus G_o (KPa)	Long-term Shear Modulus G_∞ (KPa)	Decay Constant β (sec^{-1})
White Matter	41.0	7.8	700
Gray Matter	34.0	6.4	700

Computer Simulation Code

The head model and associated constitutive models were imported and defined in the shock physics computer wave code CTH [25]. CTH is an Eulerian, finite volume computer code that is capable of tracking up to 20 materials, simulating their interactions and material response as they undergo impact, blast loading, and penetration. Due to the Eulerian nature of the solution scheme in CTH, the code is able to account for large strain deformations and flow distortions without need for periodic redefinition of the computational mesh, as is required of finite element codes. A wide variety of nonlinear equation-of-state (EOS) and constitutive models describing strength and fracture behavior are available for use within CTH to describe complex material response during impact and blast wave loading.

Blast Simulations

Simulations of direct blast exposure of the head were conducted from three principal directions, anterior (front), posterior (rear), and lateral (right side). The simulation results were analyzed to identify and map sites within the brain experiencing high levels of stress and wave energy. We also investigated the influence of doubling the blast strength from two of the three directions: anterior and lateral.

We selected blast conditions within the marginal limits of pressure and pulse width for threshold lung damage, defined by the corrected Bowen survivability curve for primary blast injury [26]. We chose these conditions to investigate blast injury scenarios that were otherwise predicted to be survivable. These blast conditions were equivalent to those predicted for a location 2 to 3 meters distant from a detonated explosive device constructed from a 3 kg charge of Octol explosive.

Our blast scenarios were simulated by first positioning the head model in an atmosphere of air at ambient conditions. A slab of energized air, held at conditions of elevated energy and pressure, was positioned 16 cm from the head at time zero. At times greater than zero, mass flow was permitted to occur from the slab of energized air thereby generating a blast wave. The amplitude and pulse width of the blast wave was determined by setting the energized air to predefined conditions of energy, pressure, and slab thickness. This procedure was employed to generate a blast wave of 1.3 MPa (13 bars) magnitude propagating through ambient air in the direction of the head model. The structure of this blast wave is illustrated in Figure 2.

The blast wave was permitted to envelop the head before being absorbed by transmitting boundary conditions positioned downstream from the head. A typical blast simulation required 31 hours using 64 processors on the Sandia National Laboratories Thunderbird computer to integrate out to a time of 2 ms for a 16.72 million cell calculation.

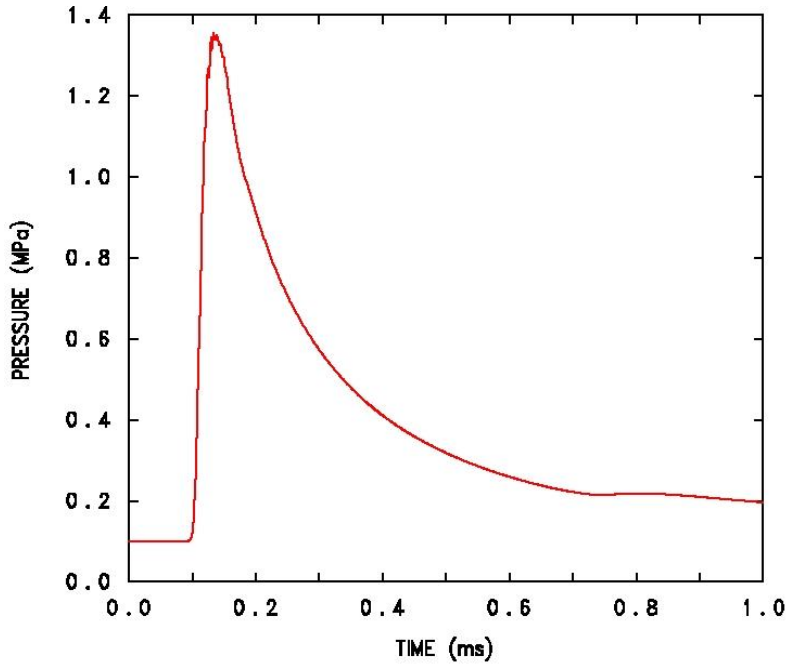

Figure 2. Air blast wave structure of 1.3 MPa (13 bars) magnitude.

Results

Each simulation data set tracked 3-dimensional calculations of maximum values of pressure, volumetric tension, and deviatoric (shear) stress. In addition, we placed Lagrangian tracer points for time histories at locations we deemed important to check whether they measured significant stress levels. Tracer points were positioned, for example, in the corpus callosum, internal capsule, anterior temporal, and at gray matter-white matter junctions.

Three orientations of blast simulation were carried out to 2 ms each. This time interval was selected by observing that the majority of the intracranial wave mechanics had played out by that time and the associated stress peaks had been established. Figure 3 shows plots of maximum pressure and volumetric tension reached in a mid-ventricular axial plane over the 2 ms simulation time. Note that the regions of highest pressure directly correlated with closest proximity to the blast source. Regions of maximum volumetric tension occurred primarily at sites opposite to the blast source, sometimes referred to as the contrecoup site. Figure 4 shows similar plots of maximum pressure and tension in a mid-sagittal plane. Maximum pressures between 3 to 4 MPa (30 to 40 bars) consistently occurred on the blast side of the head, while maximum tensions up to 0.8 MPa (8 bars) were observed on the contralateral side.

Comparisons of deviatoric stress in coronal sections between the three blast orientations are presented in Figure 5. The approximate locations of the coronal sections are shown by the horizontal dashed lines in the first axial image of Figure 3. The most anterior slice at 15.5 cm (row A) shows differences in shear distributions between anterior, posterior and lateral blasts. The coronal slice at 12 cm (row B) displays elevated shear stress in the temporal lobes and in cortical areas (black arrows) for both anterior and posterior blast orientations. In the lateral blast scenario, elevated shear was diffusely distributed in the right hemisphere closest to the blast source, compared to the contralateral hemisphere (red arrows). The coronal slice at 8 cm (row C) includes parietal and temporal lobes and passes through the posterior horns of the lateral ventricles. In this plane there were similar shear stress distributions from anterior and posterior blast orientations. The highest levels of shear stress occurred in the inferior regions and cortical areas at the gray-white junctions (arrows). In contrast, prominent focal areas of high shear stress developed in the lateral blast scenario (red oval). Row D images at 4.5 cm represent the coronal plane located in the posterior brain region including the cerebellum and occipital lobes. Focal areas of elevated shear stress in this slice occurred more prominently with anterior blast (red box) while overall shear levels were generally higher throughout the slice in the posterior blast scenario (red arrow).

The three dimensional complexity of shear stress distribution can be appreciated by observing Figure 6 along with Figure 5. Figure 6 shows areas of maximum shear stress in the same mid-ventricular axial plane as that displayed in Figure 3 and the same mid-sagittal plane displayed in Figure 4. The axial sections (row A) show considerable differences in shear localization in all three blast scenarios. More focal areas of elevated shear were seen in the lateral blast scenario (red oval) whereas the anterior corpus callosum showed greater overall shear in the anterior blast (black arrow) but focal shear localizations in the posterior blast (red arrows). The occipital area (short arrow) was most affected in the posterior blast scenario. In the mid-sagittal views (row B), all blast orientations generated higher shear in the sub-frontal regions (red ovals) and brainstem areas. Posterior blast was the only orientation generating high shear stress levels near the midline occipital region (arrow).

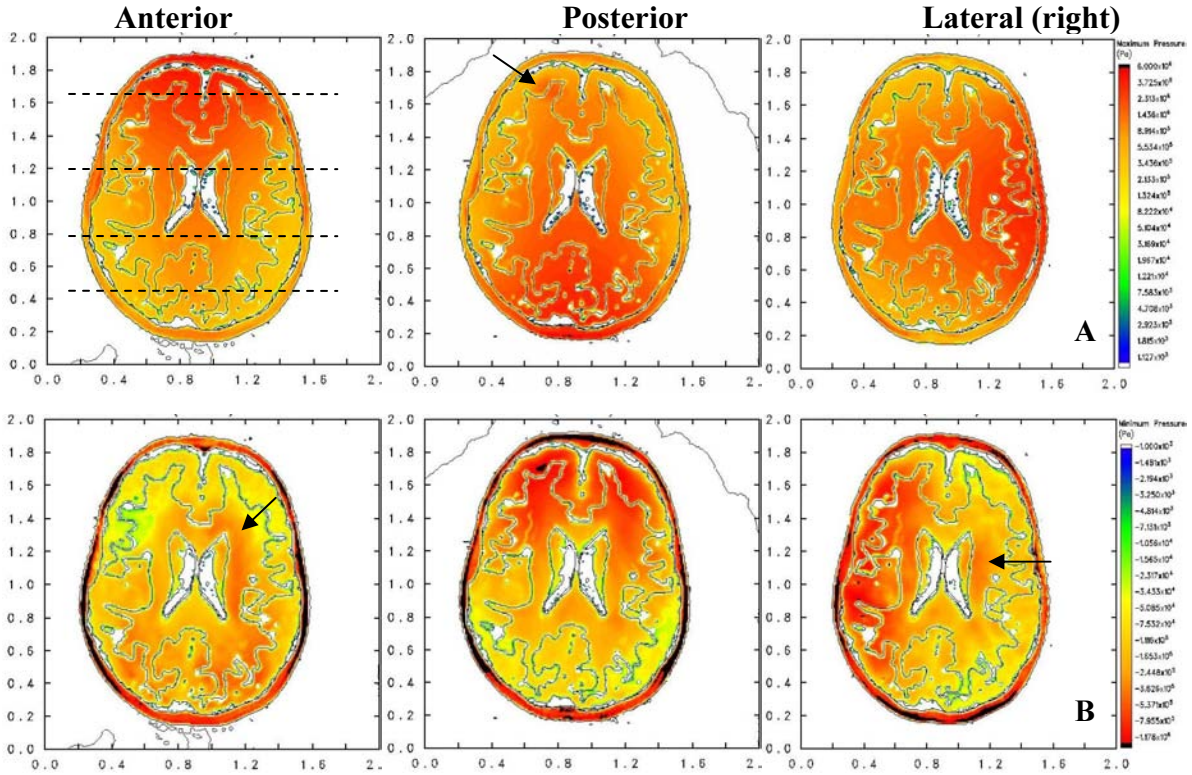

Figure 3. Maximum pressure (row A) and volumetric tension (row B) in a mid-ventricular axial plane for anterior, posterior, and right lateral blast orientations. Scale: row A: blue = 1 KPa, red = 6 MPa; row B: blue = 1 KPa, red = 1.2 MPa.

Time-resolved histories of pressure, volumetric tension, and deviatoric stress were recorded at the material locations associated with each of the tracer points. Because the tracer locations had to be specified before the simulation was run, many of them were placed in regions different from those experiencing maximal stress levels in the subsequent calculations. However, several of the tracer point histories were highly revealing. Four such tracer histories occurred for points 64 through 67, positioned in a brain slice (Figure 7) located below the lateral ventricles and passing through temporal and frontal lobe regions. The axial position of this slice is denoted by the horizontal dashed line displayed in the upper left image of Figure 4. Pressure and shear stress data from these tracer points are shown in Figures 8 and 9. For all tracer points in these figures, the shear stress continues to evolve over 2 ms, compared to the much more transient pressure wave interactions, which are played out within 0.8 milliseconds.

Differences in peak pressure timing reflect the varying distances from blast origin to each tracer point. Oscillations or ringing of the pressure wave is prominent, with tracer points 64 and 65 also experiencing significant volumetric tension (negative pressures) up to 0.4 MPa. As noted previously, regions of maximum pressure developed on the side closest to the blast and were highest in the lateral blast scenario. The nominal peak pressure of the blast wave prior to interaction with the skull was 1.3 MPa. However, as a result of differences in acoustic impedance between the air and skull, the pressure wave shocks up to a value of over 4 MPa at the air-skull interface. The difference in acoustic impedances between the skull and brain causes the pressure wave to reduce in strength somewhat as the wave propagates into the brain where it is observed that the maximum pressure at tracer point 67 is 2.7 MPa in the lateral blast scenario (Figure 9).

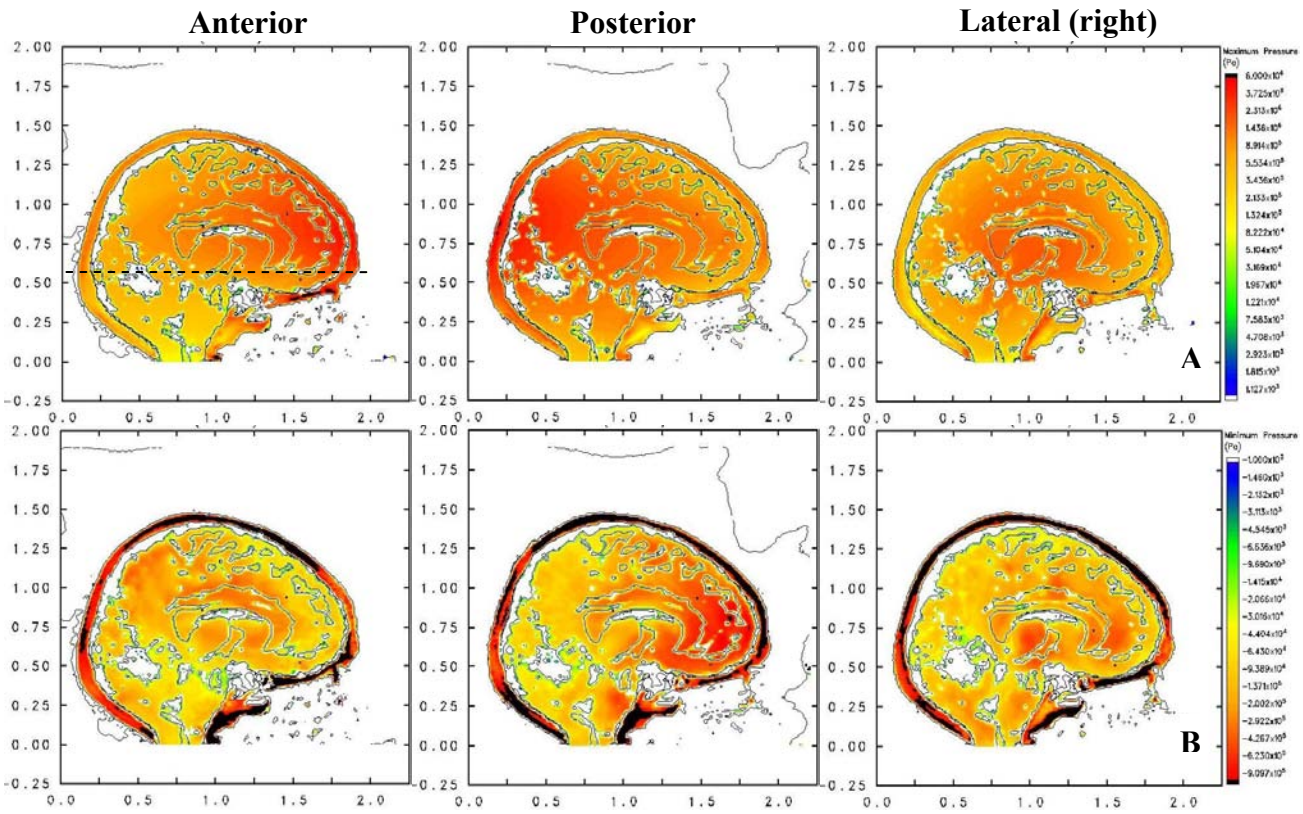

Figure 4. Maximum pressure (row A) and volumetric tension (row B) in a mid-sagittal plane for anterior, posterior, and right lateral blast orientations. Scale: row A: blue = 1 KPa, red = 6 MPa; row B: blue = 1 KPa, red = 0.9 MPa.

The even numbered tracers (64 & 66) were positioned in the left hemisphere and odd numbered tracers (65 & 67) in the right (Figure 7). Frontal lobe tracers 64 and 65 experienced the highest shear from anterior blast (red curves, Figure 8) while temporal lobe tracers 66 and 67 experienced maximal shear from lateral blast (blue curves, Figure 9). Left-right asymmetry occurred in the maximum shear stress at frontal lobe tracers 64 (3.4 KPa) and 65 (~6 KPa) from anterior blast. In contrast, left-right asymmetry occurred in the maximum shear at temporal lobe tracers 66 (1.5 KPa) and 67 (0.58 KPa) from lateral blast.

Discussion

We have conducted a modeling and simulation investigation of the wave motion that occurs within the human brain as a result of blast loading to the head. The results predict significant levels of pressure and deviatoric (shearing) stress occurring at focal regions in the brain within the first 2 milliseconds of the blast event. To our knowledge, this is the first report of a modeling and simulation investigation of blast-induced intracranial wave phenomena at earlier times.

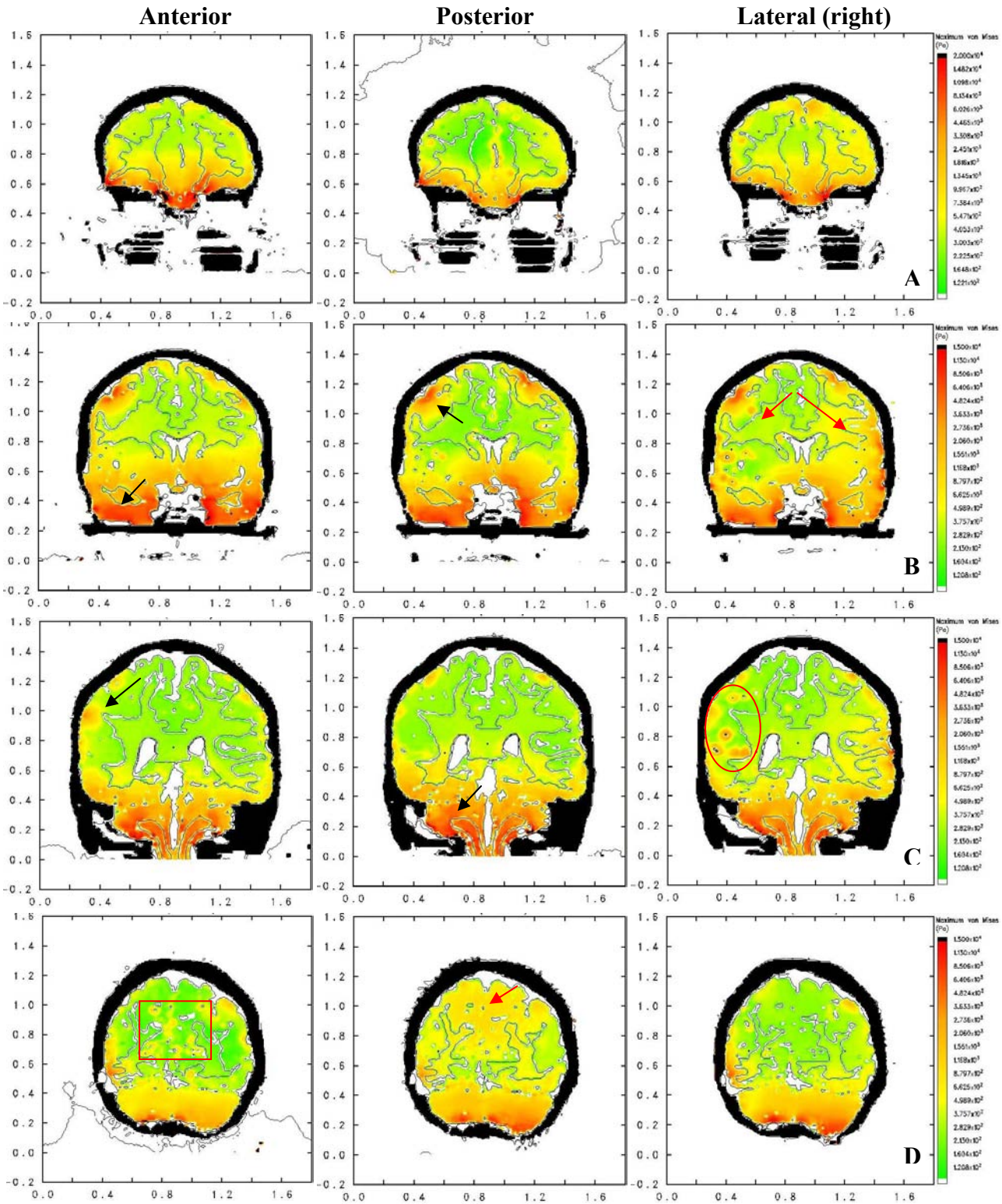

Figure 5. Maximum deviatoric stress in representative coronal planes for anterior, posterior, and right lateral blast orientations. Scale: (all rows): blue = 0.1 KPa, red = 15 KPa. Rows A-D correspond to the horizontal dashed lines appearing in the upper left axial image of Figure 3.

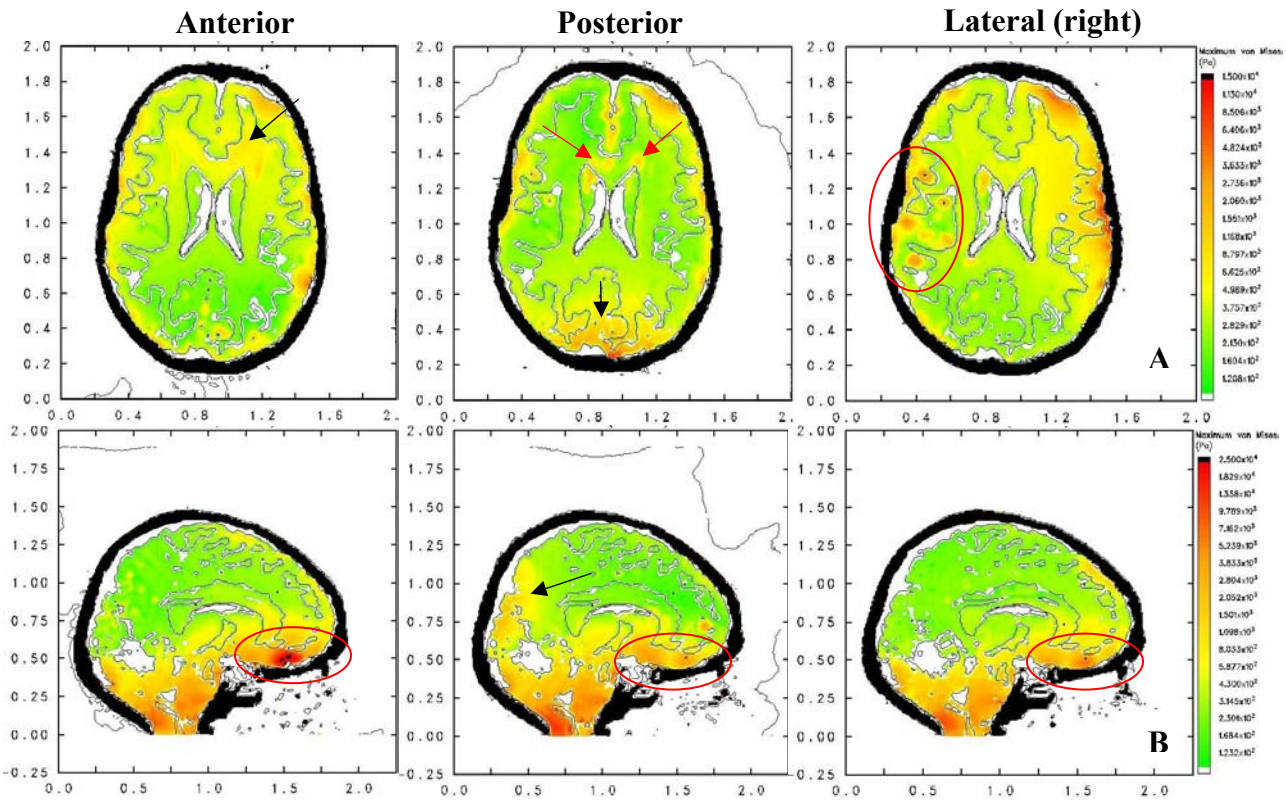

Figure 6. Maximum deviatoric (shear) stress in a mid-ventricular axial plane (row A) and mid-sagittal plane (row B) for anterior, posterior, and right lateral blast orientations. Scale: row A: blue = 0.1 KPa, red = 15 KPa; row B: blue = 0.1 KPa, red = 25 KPa.

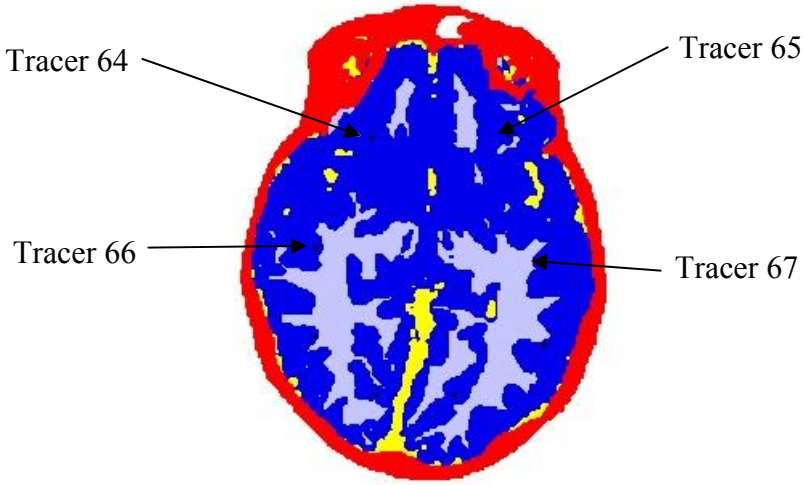

Figure 7. Tracer point examples in an axial slice below the lateral ventricles, passing through frontal and temporal lobes. The axial position of this slice is identified by the horizontal dashed line in the upper left image of Figure 4. Red = skull bone, dark blue = gray matter, light blue = white matter, yellow = cerebral spinal fluid (CSF).

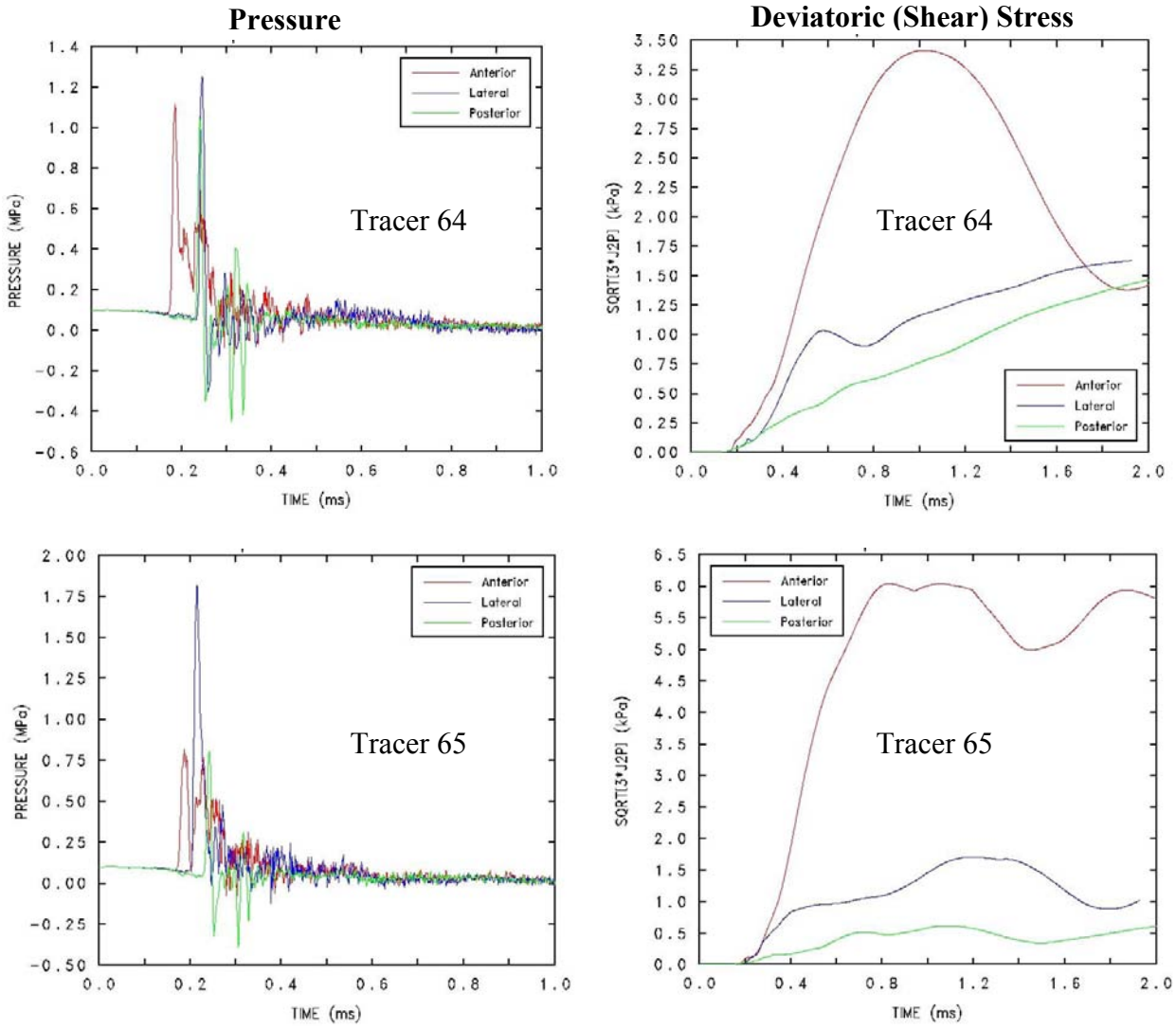

Figure 8. Pressure (left) and deviatoric stress (right) at tracer locations 64 and 65 located in the frontal lobes of the axial slice in Figure 7. Red = anterior, blue = lateral, and green = posterior. The y-axis labels for the deviatoric stress plots denote von Mises stress.

A study conducted by Zhang, et al. [27], of football collisions predicted shear stress levels of 3.1-6.4 KPa (mean of 4.5 KPa) in the thalamus that were associated with concussive injury and mild TBI. If these impact calculations represent an injury threshold for shear stress, then we predict that the stress levels we calculated for the brain from wave motion alone may be significant. Furthermore, our simulations imply that blast-induced shear stresses develop on a time-scale shorter than that associated with the intracranial accelerations typically linked to TBI, where significant translational and rotational accelerations tend to develop over a range of 5-20 milliseconds [28]. Lastly, our results suggest that shear waves of significant magnitude are generated within the head due to the presence of the skull which possesses significant shear strength and wave mode conversion, at material boundaries and interfaces, of the purely volumetric blast wave into intracranial waves comprised of both volumetric and deviatoric (shear) components.

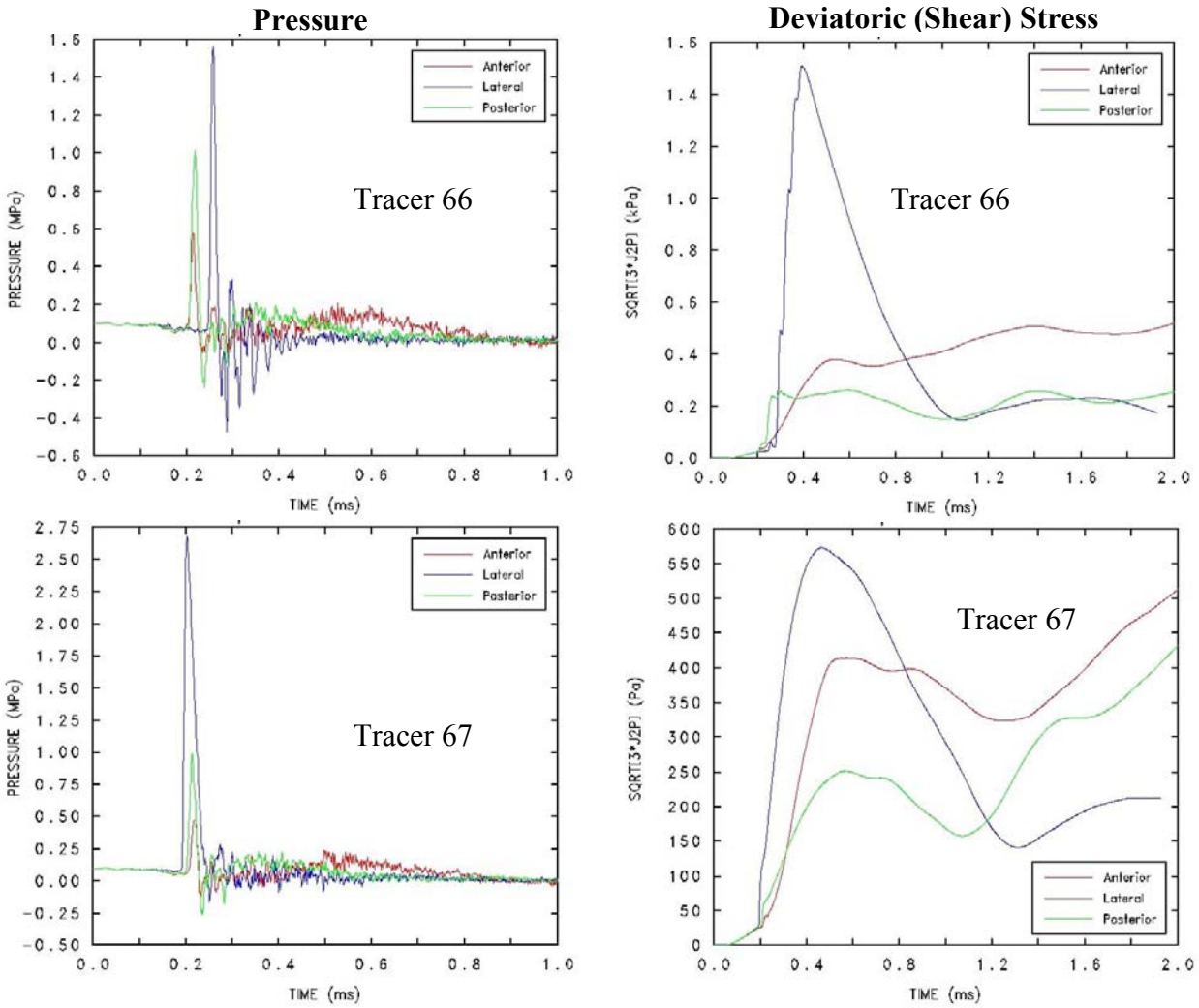

Figure 9. Pressure (left) and deviatoric stress (right) at tracer locations 66 and 67 located in the temporal lobes of the axial slice in Figure 7. Red = anterior, blue = lateral, and green = posterior. The y-axis labels for the deviatoric stress plots denote von Mises stress.

Although there appears to be no correlation of pressure with axonal injury in the literature, our blast simulations predict significant blast pressure magnification (~ 3-fold magnification) once the pressure waves have transited through the skull and into the brain. The simulations also show that these pressure waves introduce pressure and subsequent volumetric tension to brain tissue over brief periods of time (~ 0.1-0.2 ms). If these brief but relatively high magnitude pressure–tension excursions actually occur as a result of blast loading, then they may represent an additional mechanism for axonal damage.

We also conducted simulations of anterior and posterior blast loading to the head with a blast wave possessing double the strength of the 1.3 MPa wave depicted in Figure 2. For these cases, the blast wave displayed a pulse width similar to that of the 1.3 MPa wave, but with an amplitude of 2.6 MPa. The resulting stress distributions predicted in these simulations occurred in the same brain regions as seen in the 1.3 MPa blast scenarios but with the resulting pressure and deviatoric stress levels approximately doubled.

This investigation predicted wave motion and stresses on time scales significantly shorter than those calculated in other investigations of impulse loading to the head [29-33]. The explanation for this important observation has two parts. First, the degree of resolution of our computational mesh is significantly greater and, second, the solution algorithms employed in our simulation code CTH are explicit in nature. In our current simulation study, we are using a head model (illustrated in Fig. 1) that is resolved into 1 mm cubic voxels, totaling a little over 6.7 million computational cells. The surrounding air in our blast simulations is also represented at a 1 mm resolution. The solution scheme implemented in CTH is explicit in nature, employing an integration time step that is constrained by the Courant condition [34] to be less than the transit time of the fastest wave disturbance across the smallest cell dimension in the calculation. For the simulation results presented here, the time step was calculated to be a little less than 200 nanoseconds (~2.0E-7 sec). At this time step, wave disturbances on the order of 1 MHz can be resolved. Consequently, the solution scheme employed by CTH possesses the ability to resolve wave disturbances that exist at significantly shorter timescales than those resolved by solution methods based on implicit solution techniques or employing larger cell or element sizes [35].

A considerable body of work exists on experimental models and computer simulations of impact loading to the head [30;31;36-44]. These studies have established the role of brain accelerations in the development of diffuse axonal injury and its consequences. Based on the present study, we believe that early time wave action will also occur after blunt impact and may contribute to the overall injury associated with TBI by that mechanism. This possibility is supported by our preliminary study of impact to the head [45]. One of the interesting questions related to mild and moderate TBI is why the outcomes can be so different between patients with similar severity of injury, loss of consciousness, or initial Glascow Coma Scale score. Even TBI patients with normal conventional brain MRI scans can suffer enduring disability in memory, information processing, and other cognitive domains. Why does one TBI patient return to normal life activities without obvious sequelae while a similarly injured subject does not? One explanation could be that eloquent areas of the brain or critical connections are either damaged or spared at the microscopic level. The evolution of post impact or blast wave action, influenced by complex individual head geometry and tissue interfaces, might explain some of the variability in outcome. This mechanism is especially plausible in injuries involving little or no head motion, for example assaults with blunt objects and perhaps primary blast.

Our calculations represent an initial step in exploring the role of wave action at early times in the development of axonal injury after blast or impact loading. The head model used in this study possesses high resolution and incorporates constitutive models with associated properties for 5 constituent materials. The high resolution of the model allows our calculations to resolve the early time evolution of wave action that would not be possible with the larger size of volume elements used in typical finite element calculations. However, our head model currently lacks several structures likely to be important to improving the fidelity of the simulations and validating the predictions with actual brain injury metrics. For example, our model currently does not include the tentorial membranes and falx. Both of these tough fibrous structures would represent an interface and physical boundary separating left and right hemispheres and cerebral from infratentorial structures. Furthermore, we have modeled the biological materials as homogeneous and isotropic. However, this is not the case for the boney material of the skull and the white matter tracks (e.g., corpus callosum) of the brain. In future studies we plan to improve our head model to include the intracranial membranes as well as to account for porosity of the skull and anisotropy of the white matter tissue.

A better understanding of the physical mechanisms underlying TBI is critical to the development of mitigation strategies involving the design of helmets and other protective gear. The role of intracranial wave action may need to be considered in such armor designs. A reliable, validated simulation method for blast and impact injury would clearly facilitate the development of protection strategies for the unlimited range of injury scenarios. It would be impossible to replicate each injury mechanism experimentally.

In summary, we have conducted simulations of blast injury to the human head and calculated the evolution of intracranial wave action over the first 2 ms after blast exposure. Our results suggest that significant levels of pressure, volumetric tension, and shear stress can occur in focal areas of the brain, dependent on the orientation of the blast wave and the complex geometry of the skull, brain, and tissue interfaces. The focal development of stress or strain energy could exceed the threshold for axonal injury and contribute to the development of TBI and its neurological consequences. If the significance of this early time mechanism is confirmed, the current understanding of the mechanisms for TBI will need to be modified to include this phenomenon, in addition to the later time brain accelerations and rotations commonly thought to underlie axonal injury.

This Page Intentionally Left Blank

References

1. Centers for Disease Control and Prevention. http://www.cdc.gov/ncipc/pub-res/TBI_in_US_04/TBI_ED.htm. CDC . 2007.
   Ref Type: Electronic Citation

2. Fischer, H., 2007. United States Military Casualty Statistics: Operation Iraqi Freedom and Operation Enduring Freedom. Congressional Research Service report, RS22452.

3. Warden, D., 2006. Military TBI during the Iraq and Afghanistan wars. J. Head Trauma Rehabil., 21(5): 398-402.

4. DePalma, R.G., Burris, D.G., Champion, H.R., and Hodgson, M.J., 2005. Blast injuries. N. Engl. J. Med., 352(13): 1335-1342.

5. Taber, K.H., Warden, D.L., and Hurley, R.A., 2006. Blast-related traumatic brain injury: what is known? J. Neuropsychiatry Clin. Neurosci., 18(2): 141-145.

6. Buki, A. and Povlishock, J.T., 2006. All roads lead to disconnection?--Traumatic axonal injury revisited. Acta Neurochir. (Wien.), 148(2): 181-193.

7. Smith, D.H., Meaney, D.F., and Shull, W.H., 2003. Diffuse axonal injury in head trauma. J. Head Trauma Rehabil., 18(4): 307-316.

8. Adams, J.H., Graham, D.I., Murray, L.S., and Scott, G., 1982. Diffuse axonal injury due to nonmissile head injury in humans: an analysis of 45 cases. Ann. Neurol., 12(6): 557-563.

9. Graham, D., Gennarelli, T., and McIntosh, T., 2002. Trauma. In: D.Graham and P.Lantos (Editors), Greenfield's Neuropathology, Vol. 2. Arnold, Hodder Headline Group, London.

10. Smith, D.H., Chen, X.H., Xu, B.N., McIntosh, T.K., Gennarelli, T.A., and Meaney, D.F., 1997. Characterization of diffuse axonal pathology and selective hippocampal damage following inertial brain trauma in the pig. J. Neuropathol. Exp. Neurol., 56(7): 822-834.

11. Strich, S., 1961. Shearing of Nerve Fibers as a cause of Brain Damage due to Head Injury: A Pathological Study of Twenty Cases. Lancet, 2: 443-448.

12. Smith, D.H., Chen, X.H., Xu, B.N., McIntosh, T.K., Gennarelli, T.A., and Meaney, D.F., 1997. Characterization of diffuse axonal pathology and selective hippocampal damage following inertial brain trauma in the pig. J. Neuropathol. Exp. Neurol., 56(7): 822-834.

13. Buki, A. and Povlishock, J.T., 2006. All roads lead to disconnection?--Traumatic axonal injury revisited. Acta Neurochir. (Wien.), 148(2): 181-193.

14. Povlishock, J.T. and Katz, D.I., 2005. Update of neuropathology and neurological recovery after traumatic brain injury. J. Head Trauma Rehabil., 20(1): 76-94.

15. Buki, A. and Povlishock, J.T., 2006. All roads lead to disconnection?--Traumatic axonal injury revisited. Acta Neurochir. (Wien.), 148(2): 181-193.

16. Povlishock, J.T., Becker, D.P., Cheng, C.L., and Vaughan, G.W., 1983. Axonal change in minor head injury. J. Neuropathol. Exp. Neurol., 42(3): 225-242.

17. Povlishock, J.T. and Katz, D.I., 2005. Update of neuropathology and neurological recovery after traumatic brain injury. J. Head Trauma Rehabil., 20(1): 76-94.

18. Reeves, T.M., Phillips, L.L., and Povlishock, J.T., 2005. Myelinated and unmyelinated axons of the corpus callosum differ in vulnerability and functional recovery following traumatic brain injury. Exp. Neurol., 196(1): 126-137.

19. Nakayama, N., Okumura, A., Shinoda, J., Yasokawa, Y.T., Miwa, K., Yoshimura, S.I., and Iwama, T., 2006. Evidence for white matter disruption in traumatic brain injury without macroscopic lesions. J. Neurol. Neurosurg. Psychiatry, 77(7): 850-855.

20. Rugg-Gunn, F.J., Symms, M.R., Barker, G.J., Greenwood, R., and Duncan, J.S., 2001. Diffusion imaging shows abnormalities after blunt head trauma when conventional magnetic resonance imaging is normal. J. Neurol. Neurosurg. Psychiatry, 70(4): 530-533.

21. The Visible Human Project. http://www.nlm.nih.gov/research/visible/visible_human.html. National Library of Medicine . 2007.
Ref Type: Electronic Citation

22. Black, J. and Hastings, G., 1998. Handbook of Biomaterial Properties. Chapman & Hall Publishing, London, UK.

23. Zhang, L., Yang, K.H., and King, A.I., 2001. Comparison of brain responses between frontal and lateral impacts by finite element modeling. J. Neurotrauma, 18(1): 21-30.

24. Hertel, E. and Kerley, G. CTH Reference Manual: The Equation of State Package. 1998. Sandia National Laboratories report SAND98-0947, Albuquerque, NM.
Ref Type: Report

25. Hertel, E., Bell, R., Elrick, M., Farnsworth, A., Kerley, G., McGlaun, J., Petney, S., Silling, S., and Taylor, P., 1993. CTH: A Software Family for Multi-Dimensional Shock Physics Analysis. Proceedings of the 19th International Symposium on Shock Waves, 1: 377-382.

26. Gruss, E., 2006. A Correction for Primary Blast Injury Criteria. J. Trauma Injury, Infection, and Critical Care, 60: 1284-1289.

27. Zhang, L., Yang, K.H., and King, A.I., 2004. A proposed injury threshold for mild traumatic brain injury. J. Biomech. Eng, 126(2): 226-236.

28. Viano, D.C., Casson, I.R., Pellman, E.J., Bir, C.A., Zhang, L., Sherman, D.C., and Boitano, M.A., 2005. Concussion in professional football: comparison with boxing head impacts--part 10. Neurosurgery, 57(6): 1154-1172.

29. Horgan, T. and Gilchrist, M., 2004. Influence of FE Model Variability in Predicting Brain Motion and Intracranial Pressure Changes in Head Impact Simulations. International Journal of Crashworthiness, 9: 401-418.

30. Nishimoto, T. and Murakami, S., 2000. Direct Impact Simulations of Diffuse Axonal Injury by Axial Head Model. JSAE Review, 21: 117-123.

31. Suh, C., Kim, S., and Hwang, B., 2005. Finite Element Analysis of Brain Damage due to Impact Force with a Three Dimensional Head Model. Advances in Fracture Strength, Parts 1-4, 297-300: 1333-1338.

32. Willinger, R., Kang, H.S., and Diaw, B., 1999. Three-dimensional human head finite-element model validation against two experimental impacts. Ann. Biomed. Eng, 27(3): 403-410.

33. Zhang, L., Yang, K.H., and King, A.I., 2001. Comparison of brain responses between frontal and lateral impacts by finite element modeling. J. Neurotrauma, 18(1): 21-30.

34. Courant, R., Friedrichs, K., and Lewy, H., 1967. On the Partial Difference Equations of Mathematical Physics. IBM Journal, March: 215-234.

35. Lapidus, L. and Pinder, G., 1982. Numerical Solutions of Partial Differential Equations in Science and Engineering. Wiley Publishing, New York, NY.

36. King, A.I., 1993. Progress of research on impact biomechanics. J. Biomech. Eng, 115(4B): 582-587.

37. King, A.I., Ruan, J.S., Zhou, C., Hardy, W.N., and Khalil, T.B., 1995. Recent advances in biomechanics of brain injury research: a review. J. Neurotrauma, 12(4): 651-658.

38. Ruan, J.S., Khalil, T., and King, A.I., 1991. Human head dynamic response to side impact by finite element modeling. J. Biomech. Eng, 113(3): 276-283.

39. Ruan, J.S., Khalil, T., and King, A.I., 1994. Dynamic response of the human head to impact by three-dimensional finite element analysis. J. Biomech. Eng, 116(1): 44-50.

40. Willinger, R., Kang, H.S., and Diaw, B., 1999. Three-dimensional human head finite-element model validation against two experimental impacts. Ann. Biomed. Eng, 27(3): 403-410.

41. Zhang, L., Yang, K.H., and King, A.I., 2001. Comparison of brain responses between frontal and lateral impacts by finite element modeling. J. Neurotrauma, 18(1): 21-30.

42. Zhou, C., Khalil, T., and King, A.I., 1994. Shear Stress Distribution in the Porcine Brain due to Rotational Impact. Proceedings of the 38th Stapp Car Crash Conference, SAE paper no. 942214, Society of Automotive Engineers, Inc: Warrendale, PA: 133-143.

43. Zhou, C., Khalil, T., and King, A.I., 1995. A New Model Comparing Impact Response of the Homogeneous and Inhomogeneous Human Brain. Proceedings of the 39th Stapp Car Crash Conference, SAE paper no. 942214, Society of Automotive Engineers, Inc: Warrendale, PA: 121-137.

44. Zong, Z., Lee, H.P., and Lu, C., 2006. A three-dimensional human head finite element model and power flow in a human head subject to impact loading. J. Biomech., 39(2): 284-292.

45. Taylor, P. and Ford, C., 2007. Simulation of Early-Time Head Impact leading to Traumatic Brain Injury. International NeuroTrauma Letter of the International Brain Injury Association, http://www.internationalbrain.org/enews/issue1_07/index.html.

Distribution

Internal Distribution

1	MS 0321	J. Peery, 1400
1	MS 0321	J. Mitchiner, 1430
1	MS 0351	R. Stulen, 1000
1	MS 0370	J. Strickland, 1433
1	MS 0378	R. Summers, 1431
1	MS 0378	M. Kipp, 1431
1	MS 0484	R. Skocypec, 8000
1	MS 0724	J. Nelson, 6060
1	MS 1005	A. Nanco, 6345
1	MS 1005	G. Sleefe, 6340
1	MS 1164	W. Guyton, 5400
1	MS 1188	J. Wagner, 6341
1	MS 1322	J. Aidun, 1435
20	MS 1322	P. Taylor, 1435

1	MS 0123	D. Chavez, LDRD Office, 1011 (electronic copy)
1	MS 0899	Technical Library, 9536 (electronic copy)


Sandia National Laboratories